PAPER

Effects of confinement, surface-induced orientations and strain on dynamical behaviors of bacteria in thin liquid crystalline films†

Peter C. Mushenheim,[a] Rishi R. Trivedi,[b] Susmit Singha Roy,[c] Michael S. Arnold,[c] Douglas B. Weibel[b] and Nicholas L. Abbott*[a]

We report on the organization and dynamics of bacteria (*Proteus mirabilis*) dispersed within lyotropic liquid crystal (LC) films confined by pairs of surfaces that induce homeotropic (perpendicular) or hybrid (homeotropic and parallel orientations at each surface) anchoring of the LC. By using motile vegetative bacteria (3 μm in length) and homeotropically aligned LC films with thicknesses that exceed the length of the rod-shaped cells, a key finding reported in this paper is that elastic torques generated by the LC are sufficiently large to overcome wall-induced hydrodynamic torques acting on the cells, thus leading to LC-guided bacterial motion near surfaces that orient LCs. This result extends to bacteria within LC films with hybrid anchoring, and leads to the observation that asymmetric strain within a hybrid aligned LC rectifies motions of motile cells. In contrast, when the LC film thickness is sufficiently small that confinement prevents alignment of the bacteria cells along a homeotropically aligned LC director (achieved using swarm cells of length 10–60 μm), the bacterial cells propel in directions orthogonal to the director, generating transient distortions in the LC that have striking "comet-like" optical signatures. In this limit, for hybrid LC films, we find LC elastic stresses deform the bodies of swarm cells into bent configurations that follow the LC director, thus unmasking a coupling between bacterial shape and LC strain. Overall, these results provide new insight into the influence of surface-oriented LCs on dynamical bacterial behaviors and hint at novel ways to manipulate bacteria using confined LC phases that are not possible in isotropic solutions.

[a] Department of Chemical and Biological Engineering, University of Wisconsin-Madison, 1415 Engineering Drive, Madison, WI, 53706, USA. E-mail: abbott@engr.wisc.edu; Fax: +1-608-262-5434; Tel: +1-608-265-5278

[b] Department of Biochemistry, University of Wisconsin-Madison, 433 Babcock Drive, Madison, WI, 53706, USA. Fax: +1-608-265-0764; Tel: +1-608-890-1342

[c] Department of Materials Science and Engineering, University of Wisconsin-Madison, 1509 University Avenue, Madison, WI, 53706, USA. Fax: +1-608-262-8353; Tel: +1-608-262-3863

† Electronic supplementary information (ESI) available: Supplementary texts, Fig. S1–S6 and Videos S1–S13. See DOI: 10.1039/c5sm01489a

Introduction

When dispersed within nematic liquid crystals (LCs), micro- and nanoparticles (*e.g.*, polystyrene or silica) exhibit a range of dynamical and equilibrium behaviors that reflect the long-range orientational order and elasticity of the LC phase. For example, microparticles diffuse anisotropically and anomalously,[1–3] anisometric microparticles orient preferentially with respect to the nematic director,[4–8] and interparticle forces mediated by the elasticity of the LC induce the self-assembly of particles.[6–13] These phenomena, which have been observed for microparticles dispersed in both thermotropic[6,9–11] and lyotropic[7,12,13] LCs, reflect the strain induced in the LC phase by the presence of the particles.[14–20]

Whereas the above-mentioned studies involved synthetic 'passive' colloids dispersed in LCs, a series of recent studies have revealed that LC-mediated torques and stresses also manifest in the fundamental dynamical behaviors of living bacteria dispersed in LCs. Bacteria, which are commensurate in size to synthetic microparticles, can be dispersed in a non-toxic nematic lyotropic chromonic LC phase formed by aqueous solutions of disodium cromoglycate (DSCG) and generate flagella-derived forces that self-propel the bacteria through the LC.[21–25] Specifically, by using LC films with planar anchoring, motile, rod-shaped bacteria were observed to move parallel to the confining surfaces and to follow the nematic director (both in bulk LCs[21–23] and at isotropic-LC interfaces[24]) due to LC elastic forces and anisotropic effective viscosities in the LC. Non-motile *Proteus mirabilis* cells also were found to orient along the direction of LC alignment as a consequence of tangential LC anchoring at the cell surface.[22] Moreover, an interplay between LC-mediated intercellular forces and flagella-derived forces was shown to give rise to additional dynamic phenomena, including formation of

reversible, linear multicellular assemblies[22] and collective phenomena in concentrated dispersions of bacteria.[23] In addition to providing insight into the manner in which bacteria are influenced by anisotropic viscoelastic microenvironments encountered in biological systems (*e.g.*, aligned mucus or biopolymer solutions[26–29]), these past studies demonstrate that motile bacteria can serve as model 'active' particles in fundamental studies of anisotropic soft matter.

The interplay of LC elasticity-mediated forces and flagella-derived forces uncovered in the above-described studies with planar surface anchoring of LCs hinted to us that a potentially much broader range of behaviors of motile bacteria might emerge from changes in the alignment (and non-uniform alignment) of LCs containing bacteria. In this paper, we report an investigation of how the organization and dynamics of bacteria are altered in thin LC films confined by surfaces that cause either uniform homeotropic (perpendicular) or so-called "hybrid" anchoring of the LC (in which there is homeotropic LC anchoring at one substrate and planar anchoring at the other). Specifically, whereas a surface-induced hydrodynamic torque resulting from bacterial flagella-derived forces typically reorients and causes the motion of motile bacteria in a direction parallel to a confining surface of an isotropic solution,[30,31] we sought to determine if elastic torques generated by a homeotropically aligned LC would be sufficiently large to align and direct the motion of bacteria perpendicular to a surface (overcoming hydrodynamic, wall-induced torques). Our results support the hypothesis that elastic torques generated by surface-oriented LCs do dominate the dynamical behaviors of bacteria near LC interfaces. Indeed, based on this conclusion, we demonstrate that spatially varying profiles of the LC director, induced by confining LC films between two surfaces that anchor the LC in distinct orientations (hybrid LC films), can rectify the motion of bacteria.

In the second part of this paper, we confine bacteria in LC systems such that the small size of the LC domain does not permit the bacteria to assume an orientation that is parallel to the director. Specifically, we explore the limit where bacteria are long compared to the thickness of a homeotropic LC film. We show that, in this limit, the cells orient and move in directions orthogonal to the far-field director. Interestingly, self-propulsion of bacteria in this case creates transient distortions in the LC in the wake of each cell that have striking "comet-like" optical appearances. In addition, in this limit, we show that elastic stresses in the strained LC are sufficiently large to bend the bacteria. Interestingly, these results and others presented in this paper suggest that lyotropic LCs and bacterial systems can be mechanically matched, thus revealing a complexity in dynamical coupling (based on changes in shape of the bacteria) that has not previously been reported.

The studies reported here used motile *Proteus mirabilis* cells. *P. mirabilis* is a rod-shaped, motile, Gram-negative bacterium that can move through viscous fluids (*via* a "pushing" mechanism); genetic engineering of the cells has been performed to overexpress flagella and thus enable *P. mirabilis* to move rapidly through viscous environments.[32] Previously, we demonstrated that engineered

vegetative *P. mirabilis* cells (~3 μm in length; diameter of ~1 μm) are motile within nematic DSCG phases.[22,24] In addition, however, *P. mirabilis* is a particularly intriguing bacterium, because in response to certain environmental cues, vegetative *P. mirabilis* cells differentiate into long (10–60 μm in length; diameter of ~1 μm), multinucleate "swarm cells".[32] The density of flagella on these swarm cells is comparable to that on engineered vegetative cells overexpressing flagella, enabling the swarm cells to also move within highly viscous fluids, as well.[32]

Experimental

Bacterial strains and cell culture

P. mirabilis strain HI4320 was transformed with plasmid pflhDC to create vegetative *P. mirabilis* cells overexpressing flagella. The plasmid pflhDC contained the *flhDC* genes from *P. mirabilis* inserted into pACYC184 (which contains a gene for chloramphenicol resistance). *P. mirabilis* cells were grown in chloramphenicol-resistance nutrient medium consisting of 1% (wt/vol) peptone (Becton, Dickinson, Sparks, MD), 0.5% (wt/vol) yeast extract (Becton, Dickinson), and 1% (wt/vol) NaCl (Fisher Scientific, Fairlawn, NJ) at 30 °C in a shaking incubator.[32] Saturated overnight cultures were diluted 100-fold in 10 mL of fresh nutrient medium and grown in 150 mL Erlenmeyer flasks at 30 °C in a shaking incubator at 200 rpm. We observed that the highest swimming velocity of *P. mirabilis* cells occurred during stationary phase, hence we harvested cells at an absorbance (λ = 600 nm) of ~3.2 and concentrated them by centrifugation. The cells were washed three times with an aqueous buffer for bacterial motility (0.01 M KPO$_4$, 0.067 M NaCl, 10^{-4} M EDTA, 0.1 M glucose, and 0.001% Brig-35, pH 7.0).

Harvesting *P. mirabilis* swarm cells

P. mirabilis swarm cells were obtained according to previously published methods.[32] Briefly, we prepared swarm agar plates by pipetting 50 ml of 1.5% (wt/vol) hot swarm agar into 150 by 15 mm petri dishes. After the agar plates solidified, excess liquid was removed from the surface by storing the plates in the laminar flow hood for 20 min with the covers of the dishes ajar. To differentiate *P. mirabilis* vegetative cells into swarm cells, a swarm agar plate was inoculated with 4 μL of a suspension of 4×10^5 vegetative *P. mirabilis* cells per mL. The plate was then incubated at 30 °C at 90% relative humidity in a static incubator for 15 h. Following this incubation period, swarm cells were harvested from the smooth leading edge of a migrating colony of *P. mirabilis* cells using a 1 μL-calibrated inoculation loop.

Lyotropic LC preparation

Disodium cromoglycate (DSCG) was purchased from Sigma-Aldrich (Milwaukee, WI) and used as received. Lyotropic LCs containing DSCG were prepared by mixing 15.3 wt% of DSCG with 84.7 wt% of aqueous motility buffer. The mixture was shaken for at least 12 h to ensure complete solubility and homogeneity. At this concentration, polyaromatic DSCG molecules stack face-to-face into columnar aggregates with an

average length of 8 nm when the nematic phase is prepared in pure water.[33] In higher ionic content solutions, such as the motility buffer used to prepare our DSCG solutions, the average lengths of the aggregates may be larger than 8 nm.[34] Prior to experimentation, the DSCG solution was heated at 65 °C for 10 min to avoid possible time dependence of the properties of the mixture.[35,36] After cooling the solution to 25 °C, a small volume of motility buffer containing bacteria (either vegetative or swarm cells) was added to the DSCG mixture producing a final concentration of $\sim 10^5$ cells per μL. The final concentration of DSCG was 15.0 wt% in all experiments.

Growth of graphene monolayers *via* chemical vapor deposition (CVD)

Monolayers of graphene were grown on Cu foils (Alfa Aesar, Ward Hill, MA) as the growth catalyst. The foils were pre-cleaned with acetic acid (Fisher) for 15 min to remove contaminants and native oxides then rinsed in DI water ($\times 3$) before being dried with an air-gun. The cleaned Cu foils were then annealed for 30 min at 1030 °C in 95% argon + 5% hydrogen (340 sccm flowrate) to remove trace surface contaminants and also to reduce the surface roughness of the foil before initiating the growth process. The growth was conducted at 1030 °C with 95% argon + 5% methane (0.300 sccm) and 95% argon + 5% hydrogen (340 sccm) for 3 h in a 28 mm diameter quartz tube. The manufactured graphene on Cu foils were stored in a N_2 glovebox to prevent the oxidation of the graphene and the copper surfaces. All the graphene monolayers used for the experiments were manufactured from the same batch for consistency and the initial Raman scattering D-band (1347 cm^{-1}) to G-band (1585 cm^{-1}) intensity ratio (Fig. S1, ESI†), quantifying the defect density in the atomic membrane, varied as 0.04 ± 0.025 for the entire batch used for this study indicating a low density of defects.

Transfer of graphene onto HMDS-coated glass substrates

Graphene monolayers grown *via* CVD were transferred onto glass substrates coated with hexamethyldisilazane (HMDS) (Alfa Aesar). The transfer was completed using a commonly employed sacrificial polymer (PMMA – poly(methyl methacrylate)) method, similar to as previously reported.[37,38] CVD-graphene on copper was over-coated with PMMA (M.W. = 950k, 2% in chlorobenzene) by spin-coating at 2000 rpm. The samples were placed in copper etchant ammonium persulfate (25% Transene Company, Inc. APS-100 + 75% DI water) and then bath-ultrasonicated for 15 min to remove the bottom-facing graphene layer. The samples were left overnight (~ 10 h) in the etchant for the copper to completely etch. Post-etch, the floating PMMA on graphene was scooped out from the APS solution and re-floated in DI water ($\times 3$) to rinse any residual copper etchant. The samples were then dispersed in 5% HF in DI water for 60 min to remove trace silica particles that might have deposited from the CVD system during the growth, following which they were rinsed in DI water ($\times 3$). From the final DI water bath, the samples were scooped onto HMDS-coated glass substrates and spin-dried at 8000 rpm for 2 min to remove water trapped between the graphene sheet and the substrate. To remove

the PMMA layer, the samples were placed in room-temperature acetone baths ($\times 2$) for 20 min after which they were rinsed in isopropanol for 2 min to wash away any residual acetone. Finally, they were dried using an air-gun.

Characterization and analysis of graphene

Raman spectroscopy was performed with a MicroRaman DXRxi (Thermo Scientific) to characterize graphene monolayers grown on HMDS-coated glass substrates. A 532 nm laser with power = 3 mW, raster-scan frequency = 0.025 Hz and scan area = 50 μm × 50 μm was used to generate spatially-resolved maps for all samples. The maps were spatially-averaged and normalized to the G-band intensity to obtain the final Raman spectra. The laser spot size was focused to ~ 500 nm, and a mapping pixel size of 1 μm × 1 μm was used. Raman spectroscopy confirmed the presence of monolayers of graphene both before and after contact with a 15 wt% DSCG solution (Fig. S1, ESI†).

Preparation of imaging chambers

We created imaging chambers by adding a small volume (~ 1 μL) of 15 wt% DSCG solution on top of a glass slide between two sheets of Mylar film (10–18 μm-thick). A glass cover slip was placed on top of the Mylar and the chamber was sealed with epoxy to prevent water evaporation. To create uniform homeotropic LC films, two graphene-coated substrates were used to confine the DSCG solution.[39] In contrast, for hybrid LC films, only one of the two bounding glass substrates was coated with graphene.

Optical characterization of nematic DSCG phases

The orientation of the nematic phase of the 15 wt% DSCG solution in experimental imaging chambers was determined using plane-polarized light in transmission mode on an Olympus BX60 microscope equipped with crossed polarizers. All images were captured using a digital camera (Olympus C-2040 Zoom) mounted on the microscope and set to an f-stop of 2.8 and a shutter speed of 1/125 s.

Microscopy

We imaged cells using a Nikon Eclipse Ti inverted optical microscope equipped with crossed polarizers and a Photometrics CoolSNAP HQ2 CCD camera (Tucson, AZ) using a Nikon Plan Apo λ, 100×/1.45 oil objective lens and a Nikon S Plan Fluor ELWD 40×/0.6 objective. Videos were collected with the EM gain off and with a 90 ms exposure time (11 frames per s). Images of cells were collected using Nikon NIS Elements software.

Results and discussion

I. Homeotropic LC film; $L_{bacteria} < d_{film}$

We first characterized the manner in which vegetative *P. mirabilis* cells ($L_{bacteria} \sim 3$ μm) orient and move when dispersed in nematic LC films ($d_{film} \sim 10$ μm) confined between two graphene-coated substrates that give rise to a uniform homeotropic alignment of the LC (Table 1). While we have previously demonstrated that these

Table 1 Experimental conditions investigated in this study. Small vegetative *P. mirabilis* cells dispersed in uniform homeotropic films are investigated in Section I; long *P. mirabilis* swarm cells dispersed in homeotropic films in Section II; vegetative cells in LC films with hybrid anchoring conditions in Section III; and swarm cells dispersed in hybrid LC films in Section IV

	Bacteria cell type	
	$L \sim 3~\mu m$	$L \sim 10~\mu m - 60~\mu m$
LC film orientation		
$d \sim 10~\mu m$	I	II
$d \sim 18~\mu m$	III	IV

Fig. 1 Alignment and motility of vegetative *P. mirabilis* cells in homeotropic LC films. (A) Schematic representation of the elastic ($\Gamma_{elastic}$) and hydrodynamic ($\Gamma_{hydrodynamic}$) torques acting on a motile bacterium in a homeotropic LC film. (B) Phase contrast micrograph depicting the orientation of cells within a homeotropic LC film. The nematic director is oriented along the axis orthogonal to the plane of the page. (C) Sequence of phase contrast micrographs depicting a cell that moves back and forth across the thickness of the homeotropic film. The plane of focus remains fixed near one of the graphene-coated substrates in the micrographs. (D) Schematic (side view) depicting the handedness of the rotation of the cell body (ω_{body}) and flagella ($\omega_{flagella}$) about the axis defined by the long axis of the cell body as well as the handedness of the gyration ($\omega_{gyration}$) of the cell observed experimentally about an axis normal to the graphene-coated substrate. Scale bars = 3 μm.

motile cells orient and move parallel to the LC director in planar LC films as a result of elastic stresses that orient the cells,[22] it is well-established that hydrodynamic stresses significantly influence the behavior of motile bacteria proximate to a solid substrate. Specifically, in isotropic solutions, bacteria that swim *via* a "pushing" mechanism and establish a dipolar flow field (such as *P. mirabilis*) are attracted to surfaces by hydrodynamic interactions.[30,31] The bacteria are induced to assume an orientation in which the swimming cells align parallel to the surface due to velocity gradients in the flow field that arise in the near-surface region.[30,31] This reorientation of the cell typically occurs over a time scale of seconds when cells approach within a few micrometers of a solid substrate.[30] Inspired by these past studies, we hypothesized that vegetative cells in a homeotropic LC film and proximate to one of the confining substrates might, in contrast, adopt an orientation perpendicular to the substrate if the torque due to the elasticity of the LC ($\Gamma_{elastic}$) is sufficient in magnitude to suppress the surface-induced hydrodynamic torque ($\Gamma_{hydrodynamic}$) (Fig. 1A).

To explore this hypothesis, we first dispersed motile vegetative *P. mirabilis* in an isotropic aqueous solution confined within a $\sim 10~\mu m$-thick experimental imaging chamber. We observed in this case that the motion of the bacteria was confined predominantly within planes parallel to the substrates (using either bare glass or graphene-coated substrates), consistent with previous studies (Video S1, ESI†). Next, we dispersed vegetative cells within nematic DSCG and confined this mixture between two graphene-coated substrates separated by $\sim 10~\mu m$. We observed regions of the LC to adopt a uniform homeotropic orientation over the course of tens of minutes,[39] as confirmed by the observation of two crossed isogyres upon insertion of a sub-stage condenser and a Bertrand lens above the stage (Fig. S2, ESI†).[40] In contrast to our observations of motile bacteria in isotropic solutions, we found that motile *P. mirabilis* cells (in addition to non-motile cells) oriented approximately parallel to the direction of LC alignment within the homeotropic regions (*i.e.*, perpendicular to the graphene-coated substrates) (Fig. 1B).

To determine whether the motile vegetative *P. mirabilis* were aligning perpendicular to the bounding substrates in uniform
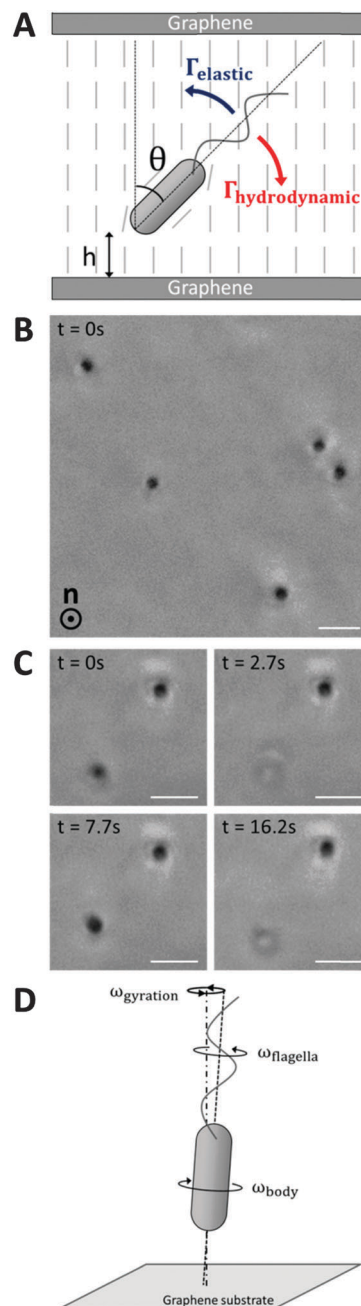
homeotropic DSCG films as a result of elastic forces, we calculated the relative magnitudes of $\Gamma_{elastic}$ and $\Gamma_{hydrodynamic}$

acting on the vegetative cells. Specifically, we calculated the elastic torque as[41,42]

$$\Gamma_{\text{elastic}} \sim \frac{4\pi K \theta L_{\text{bacteria}}}{\ln(2L_{\text{bacteria}}/R)}, \quad (1)$$

where K is the elastic constant of the LC ($K \sim 10$ pN for nematic DSCG[42]), R is the radius of a bacterium ($R = 0.5$ μm for *P. mirabilis*), and θ is the angle between the orientation of the long axis of the cell and the orientation of the far-field LC director. We estimated the hydrodynamic torque as

$$\Gamma_{\text{hydrodynamic}} \sim f_r \Omega, \quad (2)$$

where Ω is the rate (in rad s^{-1}) at which surface-induced hydrodynamic stresses cause rod-shaped bacteria to reorient and f_r is the frictional drag coefficient associated with this rotation (see ESI† for details). In the absence of other applied torques, Ω is estimated by[30]

$$\Omega \sim -\frac{3p\cos\theta\sin\theta}{64\pi\eta h^3}, \quad (3)$$

where p is the strength of the hydrodynamic force dipole, η is the viscosity, h is the distance of the bacterium away from the surface, and θ defines the angle between the cell long axis and the surface normal. For a swimming bacterium, the dipole strength can be approximated as $p \sim \eta V L_{\text{tot}}^2$,[30] where V is the linear velocity of the bacterium and L_{tot} is the total length of the bacterium (including both cell body and flagella). To compare the magnitudes of these two torques, we employed $L_{\text{tot}} = 10$ μm (a quantity that is optically measured using distortions in the LC induced by the flagella rotating behind motile bacteria[23] (Video S2, ESI†)), $\eta \sim 0.7$ Pa s as an effective viscosity of nematic 15 wt% DSCG,[22] and $V = 8.8$ μm s^{-1} as a typical velocity of vegetative *P. mirabilis* in nematic DSCG.[22] In the limit of small θ (in which the ratio $\Gamma_{\text{elastic}}/\Gamma_{\text{hydrodynamic}}$ is independent of θ), we calculate that the elastic torque associated with deviations of the alignment of a vegetative cell away from the far-field director ($\theta = 0°$) near a graphene-coated substrate ($h = 2$ μm) exceeds the wall-induced hydrodynamic torque ($\Gamma_{\text{elastic}}/\Gamma_{\text{hydrodynamic}} \sim 6$). Although our estimate of $\Gamma_{\text{hydrodynamic}}$ does not account for the anisotropic viscosities of nematic LCs,[1,3,43,44] the relative magnitudes of $\Gamma_{\text{hydrodynamic}}$ and Γ_{elastic} support our interpretation of our experimental observations in terms of the dominating influence of LC elastic torques (which overcome the influence of surface-induced hydrodynamic torques). This represents a striking departure from the typical behavior of motile rod-shaped cells near a solid substrate when dispersed in an isotropic solution.

Because we concluded that motile vegetative *P. mirabilis* cells were strongly oriented by elastic forces in homeotropic LC films, we next investigated their approach and collision with the substrates. Experimentally, we observed motile cells to remain localized for extended lengths of time (over the duration of our observations – tens of minutes) adjacent to one of the two graphene-coated substrates. The cell bodies of the five cells depicted in Fig. 1B, for example, are dynamically positioned in a single plane proximate to one of the substrates. We judged that

unidirectional flagella-derived forces were primarily responsible for this accumulation of bacteria near the bounding substrates. We note, however, that we occasionally observed vegetative cells to move back and forth along the LC director from one graphene-coated substrate to the other (Fig. 1C and Video S3, ESI†). We hypothesize that these cells are able to reverse direction due to flagella bundles that extend from both cell poles, as the elasticity of the nematic LC suppresses "tumbling" that typically reorients bacterial motion in isotropic solutions.[25]

Limited by the resolution of our optical microscope, it was difficult to establish whether the cells contacted the graphene-coated substrates by varying the focal plane, although we measured cells to regularly approach to within 1 μm from the substrates. However, we were able to conclude that bacteria did not physically adhere to the graphene-coated substrates but instead were likely dynamically positioned near the surfaces by hydrodynamic flows[31,45,46] as we observed the cell bodies of bacteria near a substrate to gyrate around an axis normal to the substrate (Fig. 1D and Video S4, ESI†). The handedness of the gyration matched that of the rotating flagella bundles (counter-clockwise when viewed from behind the cell) and proceeded at angular velocities between 1–2 rev s^{-1} (Video S5, ESI†). We measured the cell bodies of gyrating cells to deviate up to 3° away from the surface normal (see ESI† for details). Using eqn (1), we estimate that an elastic torque as large as $\Gamma_{\text{elastic}} \sim 8$ pN μm acts on the gyrating bacteria, a torque that must be balanced by rotation of the bacterial flagella. We also observed gyrating bacteria in homeotropic DSCG films with thicknesses of ~ 30 μm, suggesting this phenomenon is not simply an effect of confinement of the bacteria in LC films with $d_{\text{film}} \sim L_{\text{bacteria}}$. We note that this gyration resembles the "wobbling" of bacterial cell bodies that can occur in an isotropic solution when the long axis of a cell body and the axis of the helical flagella bundle are not collinear.[47–49]

II. Homeotropic LC film; $L_{\text{bacteria}} > d_{\text{film}}$

The results of the experiments described above establish that rod-shaped bacteria orient and move parallel to the LC director in homeotropic LC films when $L_{\text{bacteria}} < d_{\text{film}}$. Next, we investigated bacteria dispersed in a homeotropic LC film in the limit of $L_{\text{bacteria}} > d_{\text{film}}$ such that steric constraints (*i.e.*, thickness of the LC film) prevent the body of the bacterium from orienting parallel to the LC. Specifically, we dispersed *P. mirabilis* swarm cells with lengths ranging from 10–60 μm within homeotropic LC films approximately 10 μm thick. In contrast to vegetative cells, we found that swarm cells oriented and moved through homeotropic nematic DSCG films in directions orthogonal to the nematic director with a velocity of $\bar{V}_\perp = 7.5 \pm 0.3$ μm s^{-1} ($N = 97$; standard error reported) (Fig. 2A and Video S6, ESI†). This velocity is lower than that measured for swarm cells moving parallel to the director (*i.e.*, bacteria in uniform planar DSCG films; $\bar{V}_\parallel = 11.1 \pm 0.5$ μm s^{-1} ($N = 34$)) (Video S7, ESI†), consistent with the motile bacteria experiencing a higher effective shear viscosity when moving orthogonal to the director.[1–3] In support of this interpretation, we note that the ratio of the diffusion coefficients of micrometer-sized
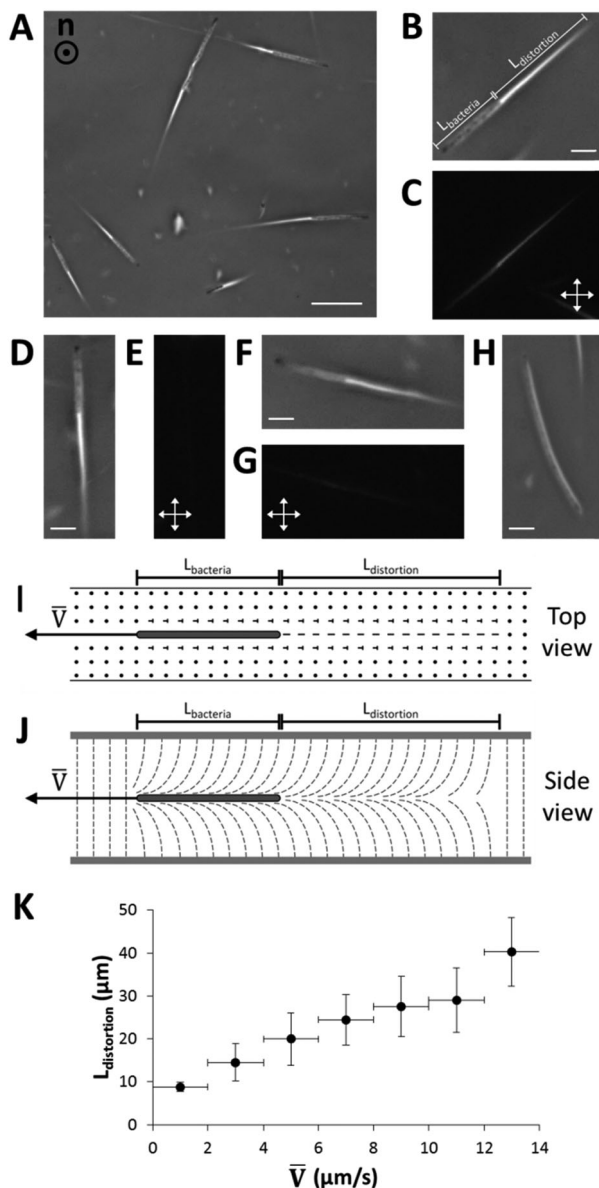
Fig. 2 Motility of *P. mirabilis* swarm cells in homeotropic LC films. (A) Phase contrast micrograph of motile swarm cells within a homeotropic LC film. The nematic director is oriented along the axis orthogonal to the plane of the page. The swarm cells move in directions orthogonal to the director, inducing distortions in the alignment of the LC in their wake. (B–G) Pairs of phase contrast micrographs (B–G) of swarm cells in homeotropic LC films taken either (B, D and F) without or (C, E and G) with crossed polarizers inserted into the optical path. In B, the length of the swarm cell body ($L_{bacteria}$) and the wake of distorted LCs ($L_{distortion}$) are denoted. (H) Phase contrast micrograph of a stationary swarm cell in a homeotropic LC film. (I and J) Schematics (I – top view; J – side view) depicting the distortion in the LC film induced by motion of swarm cells perpendicular to the director (with velocity $\bar{V}$). (K) Plot of $L_{distortion}$ as a function of $\bar{V}$ measured for 97 swarm cells in homeotropic LC films. Horizontal error bars represent intervals over which data are binned while vertical error bars represent standard deviation. Scale bar in (A) = 20 μm; scale bars in (B, D, F and H) = 5 μm.

silica particles in the nematic phase of a 13 wt% DSCG solution is $D_{\parallel}/D_{\perp} \sim 1.5$,[3] and that $\bar{V}_{\parallel}/\bar{V}_{\perp}$ for swarm cells is comparable to this value. In addition, we note that the magnitude of the

flagella-derived forces produced by bacteria may differ when the cells are oriented either parallel or orthogonal to the far-field director due, for example, to differences in the orientation of the flagella bundle relative to the cell body caused by interaction with the LC.[25]

By varying the position of the focal plane of the microscope, we determined that swarm cells (both motile and non-motile) were localized typically (but not always, see below) at or near the midplane of the homeotropic LC films (for LC films with $d_{film} < L_{bacteria}$). This observation is consistent with repulsive LC elastic forces (due to homeotropic and tangential anchoring of the LC on the graphene-coated surface and bacteria, respectively; see Fig. 2J) preventing swarm cells from approaching the graphene-coated substrates.[50–52] This observation also is a particularly interesting one because attachment to surfaces is the first step in the colonization of surfaces by bacteria (*e.g.*, in forming biofilms). These results hint that LC materials may be useful in mediating bacteria–surface interactions to minimize attachment.

We also observed that self-propulsion of swarm cells generated "wakes" that had a striking comet-like optical appearance when visualized using phase contrast microscopy due to the birefringence of the nematic DSCG (Fig. 2A and Video S6, ESI†). Although previously it was demonstrated that rotation of bacterial flagella transiently strains uniform planar DSCG films over a length scale of a few micrometers,[23] the distortions produced by swarm cells in our experiments appear to have a different origin, as we commonly measured these distortions to extend tens of micrometers behind the cell body and flagella of each swarm cell. These distortions in the LC film were long-lived, as the LC was observed to relax back to its original uniform homeotropic orientation over a time scale of seconds. By employing $\eta \sim 0.7$ Pass and $K \sim 10^{-11}$ N for nematic 15 wt% DSCG[22,43] and using a characteristic length scale of the distortions of $d_{film}/2$–5 μm, we estimated that τ, the elastic relaxation time scale ($\tau \sim \eta d_{film}^2/4K$)[53] is on the order of seconds ($\tau \sim 2$ s), consistent with our experimental observations.

To obtain additional insight into the origin of the comet-like "tails," we analyzed the motions of the swarm cells both with and without crossed polarizers (Fig. 2B–G). With crossed polarizers inserted, we found the brightness of the comet-like tails to depend on the direction of cell motion relative to the orientation of the polarizers. Specifically, whereas the wake exhibited a bright optical intensity when cells moved at an angle relative to both polarizers, appearing to reach a maximum for cells translating at approximately 45° with respect to each polarizer (Fig. 2C), the wakes were scarcely visible when cells moved nearly parallel to either polarizer (Fig. 2E and G). We note that we did not observe comparable optical signatures extending from the poles of non-motile swarm cells (Fig. 2H). These observations suggest that the motion of a swarm cell orthogonal to the homeotropically aligned nematic DSCG (in the far-field) induces a transient strain (bend and splay) within the LC, as depicted schematically in Fig. 2I and J. We measured a linear relationship to exist between the length of the LC wake ($L_{distortion}$) and the average velocity ($\bar{V}$) of each cell (Fig. 2K),

consistent with $L_{distortion}$ being determined by how far a swarm cell travels over the course of τ, the time scale that characterizes the elastic relaxation of the LC (see above).

The orientation of the LC within the wake, which relaxes over time τ, likely reflects either or both the anchoring of the LC at the surface of the cell body, and shear alignment of the LC due to the motion of the DSCG induced by the bacteria. Even in the absence of motion of the cells, as noted above and shown in Fig. 2J, the anchoring of the DSCG on the surface of the bacterial cell will induce the orientation of the LC observed within the core of the wake. In addition, however, we note that shear forces produced by the motion of the swarm cells could also lead to shear alignment of the LC in the absence of the above-described anchoring of the LC on the surface of the bacteria. This mechanism is supported by an estimate of the ratio of viscous to elastic torques, characterized by the Ericksen number ($E_r = \eta d_{film} \bar{V}/2K$),[53] which is >1 in our experiments.

We hypothesized that transient strain in the LCs induced by a moving swarm cell might also influence the motion of a second, trailing swarm cell. Consistent with this hypothesis and in support of our general physical picture proposed above, we found that when two swarm cells swam in close proximity to one another in a homeotropic LC film (in the same plane relative to the graphene-coated substrates), the trajectory of one cell, upon encountering the wake of the other cell, assumed the trajectory of the first cell (Fig. 3 and Video S8, ESI†).

Although we typically observed *P. mirabilis* swarm cells were positioned at or near the midplane of uniform homeotropic LC films, we also occasionally found motile swarm cells instead located in a plane closer to one of the two bounding graphene-coated substrates. In these cases, we found the bodies of the swarm cells to be bent along their lengths and observed the swarm cells to swim in tight, circular trajectories within the plane parallel to the substrates (Fig. 4). Moreover, when we analyzed these circular trajectories, we determined that they
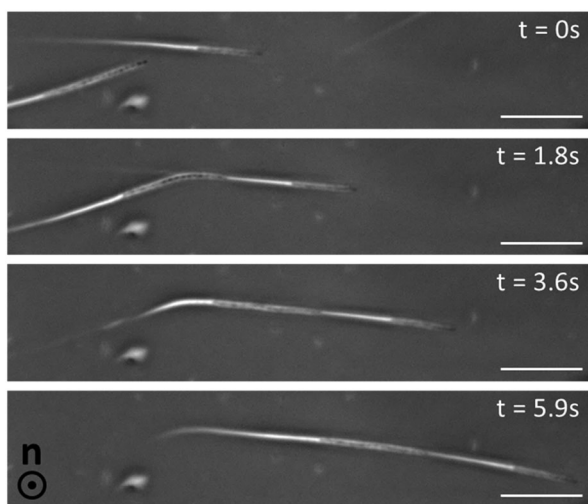

Fig. 3 Sequence of phase contrast micrographs depicting the motion of two *P. mirabilis* swarm cells within a homeotropic LC film. The trajectory of one of the cells is altered upon colliding with the wake of distorted LCs left by the other cell. Scale bars = 20 μm.
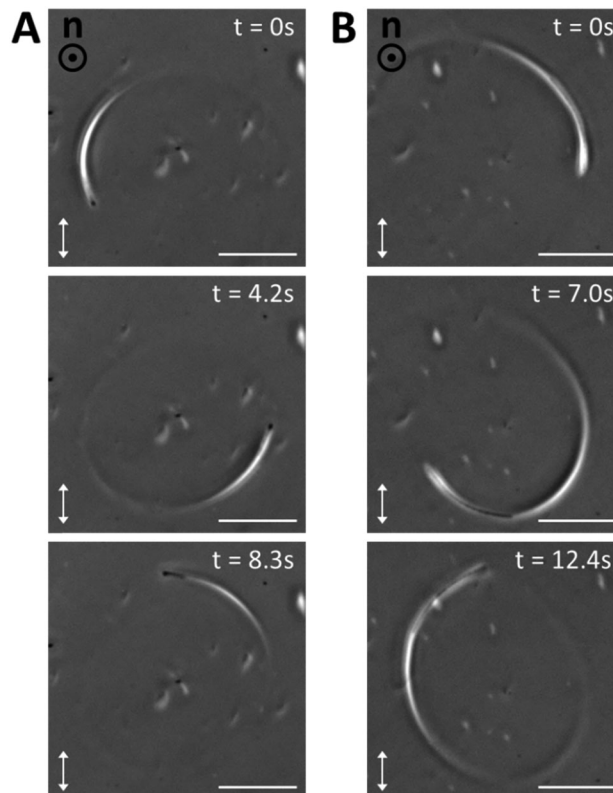

Fig. 4 Circular trajectories of swarm cells in a homeotropic LC film. (A and B) Sequences of micrographs (phase contrast with a single polarizer inserted) showing examples of the (A) counter-clockwise and (B) clockwise trajectories of motile swarm cells that arise when the cells are proximate to one of the two graphene-coated substrates in a homeotropic LC film. Scale bars = 20 μm.

always appeared counterclockwise when the cell was positioned near the graphene-coated substrate furthest from the objective of our inverted microscope (Fig. 4A and Video S9, ESI†) and clockwise when the cell was instead located near the substrate closer to the objective (Fig. 4B and Video S10, ESI†). These observations are consistent with previous reports of the emergence of circular cellular trajectories when bacteria dispersed in an isotropic solution swim near a solid surface.[31,54] These circular trajectories are caused by a wall-induced torque that arises from the motion of the cell body and the helical flagella bundle. They exhibit a specific handedness due to the chiral propulsion mechanism of the bacteria. Interestingly, however, we note that we did not observe *P. mirabilis* cells (either vegetative or swarm) to exhibit similar wall-induced circular trajectories when confined in nematic DSCG films exhibiting a uniform planar alignment. In this case, it appears that the elastic torque from the nematic LC is sufficient to suppress this wall-induced torque (analogous to the elastic suppression of vegetative cells from reorienting parallel to graphene-coated substrates when dispersed in homeotropic LC films, as described above).

III. Hybrid LC film; $L_{bacteria} < d_{film}$

A key conclusion that emerges from the above studies is that the LC elastic torques acting on bacteria near surfaces can be

sufficiently large to dominate hydrodynamic interactions that commonly govern the dynamics of bacteria in isotropic solvent systems near surfaces. To explore if the dominant influence of LC elastic stresses on bacterial dynamics near surfaces extends to situations where the director profile is non-uniform, next, we created nematic DSCG films with hybrid anchoring conditions by confining the LC between a graphene-coated substrate and a bare glass slide (Fig. S3, ESI†). In these films, the out-of-plane orientation of the LC rotates by $\pi/2$ while going from one substrate to the other. We verified that nematic DSCG films adopted this hybrid configuration by confirming (i) the extinction of transmitted light as the sample was rotated between crossed polarizers and (ii) that interference colors observed at positions of minimum extinction of the sample corresponded to lower optical retardation values than for uniform planar films of the same thickness (Fig. S3, ESI†). Consistent with this strained configuration of the LC director profile, when we dispersed small vegetative *P. mirabilis* cells within hybrid LC films, we observed that they aligned perpendicular to the graphene-coated substrate when proximate to it and parallel to the bare glass substrate when instead close to it (Fig. S4, ESI†).

Most significantly, as shown in Fig. 5, we found that when the bacteria were located in a region of the hybrid DSCG film ($d_{film} \sim 18$ μm) with a uniform in-plane orientation, the overall motion of bacteria was directed parallel to p, a vector defined by the orientation of the bend and splay distortions in the hybrid film (as shown in Fig. 5B) (Video S11, ESI†). Specifically, bacteria near the bare glass substrate within the hybrid LC film moved along the substrate in the direction parallel to p. In contrast, when a cell with flagella bundles extending from both poles reversed its direction of motion such that it was directed anti-parallel to p, the splay in the LC directed the bacterium across the thickness of the LC film towards the graphene-coated substrate, where the cell assumed an orientation approximately perpendicular to the surface. Once held in this orientation, the motion of the cell ceased until it again reversed direction, moved back towards the bare glass substrate, and then continued moving parallel to p. The net effect of this coupling between the strain of the LC and the bacteria was a rectification of the bacterial motion. Whereas rectification of bacterial motion has been achieved in isotropic solutions using microfluidic channels with special geometric features,[55,56] our results reveal that the elastic strain stored within the hybrid configuration of a nematic LC film tens of micrometers thick can also be leveraged to guide the overall motion of bacteria. Our results also demonstrate the elastic torques generated by complex and non-uniform LC director profiles also dominate hydrodynamic interactions of bacteria near surfaces. We also note that the hybrid LC films can contain "reverse domains" (see Table 1 for an example), and that future studies will investigate how bacteria navigate such domain boundaries.

IV. Hybrid LC film; $L_{bacteria} > d_{film}$

Past studies by us and others have observed bacteria dispersed in LCs to behave as rigid entities. However, the results shown in Fig. 4 clearly demonstrate that hydrodynamic interactions
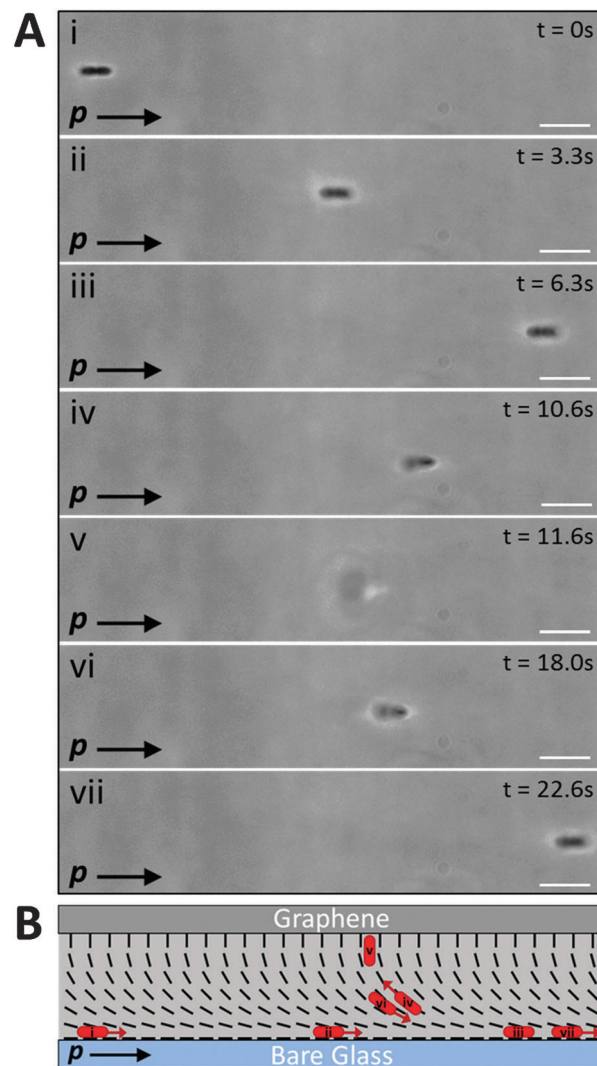

Fig. 5 Rectification of vegetative *P. mirabilis* cell motion in a hybrid LC film. (A) Sequence of phase contrast micrographs depicting the motion of a vegetative *P. mirabilis* cell within a hybrid LC film (11 μm thick). The plane of focus remains fixed near the bare glass substrate throughout the experiment. (B) Schematic representation of the director profile within the LC film along with the approximate location and direction of motion (indicated by red arrows) of the bacterium in each snapshot in A. In (A and B), p indicates the orientation of the bend and splay distortions within the hybrid LC film. Scale bars = 5 μm.

between the bacteria and surfaces can bend the bodies of swarm cells. To explore whether elastic stresses associated with strained LCs can also deform the bodies of a swarm cells, we explored LC films in which bend and splay distortions were present (in the limit $L_{bacteria} > d_{film}$). Our initial observations focused on swarm cells in hybrid DSCG films in which the direction of motion of the swarm cells was anti-parallel to p. In this situation, we observed the leading end of a swarm cell to follow the $\pi/2$ rotation of the LC director across the thickness of the film, and upon reaching the graphene-coated substrate, trapped the swarm cell in a deformed configuration in which the cell body approximately followed the director within the hybrid LC film (Fig. 6 and Video S12, ESI†). From this result, we
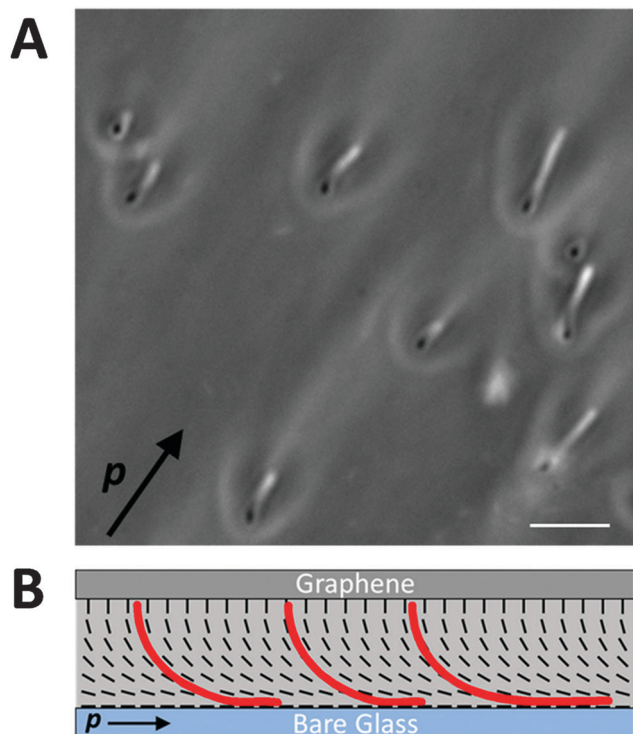
Fig. 6 Deformation of *P. mirabilis* swarm cells in hybrid LC films. (A) Phase contrast micrograph of *P. mirabilis* swarm cells dispersed within an 18 μm thick hybrid LC film (plane of focus near graphene-coated substrate). (B) Schematic representation of the director profile within the LC film along with the approximate configurations of the swarm cells. In (A and B), **p** indicates the orientation of the bend and splay distortions within the hybrid LC film. Scale bar = 10 μm.

conclude that the body of a *P. mirabilis* swarm cell is sufficiently soft that elastic stresses imparted by the LC phase can deform the cell body.

To examine further this conclusion, we compared the relative energetic cost of bending a swarm cell in a hybrid LC film (E_{cell}) to that associated with straining LCs locally around a bacterium not aligned with the far-field director (E_{LC}). We estimate the cell bending energy by the expression

$$E_{cell} = \frac{1}{2}EIL_{bend}\kappa^2, \quad (4)$$

where E is the Young's modulus, I is the second moment of inertia, L_{bend} is the arc length of and κ is the mean curvature of the deformed segment of the bent swarm cell.[57] Employing typical values for our system, we estimate $E_{cell} \sim 1 \times 10^{-17}$ J for a swarm cell with $L_{bend} = 28$ μm in a hybrid LC film 18 μm thick (see ESI† for details).

To compare the magnitude of the LC elastic energy to this value of E_{cell}, we use the expression[41]

$$E_{LC} = 2\pi LK\theta^2/\ln(2L/R) \quad (5)$$

Eqn (5) is the energetic cost associated with realigning a swarm cell of length L and radius R an angle of θ away from the far-field director in a uniformly aligned LC film. For a swarm cell with $L = L_{bend} = 28$ μm and $R = 0.5$ μm and using $K = 10$ pN,

we calculate $E_{LC} \sim E_{cell}$ when $\theta \sim 11°$. This calculation suggests that LC elastic stresses should be sufficient in magnitude to deform the body of a swarm cell, consistent with our experimental observations. Moreover, this preliminary result suggests that hybrid LC films may be useful for measurement of cell mechanical properties, particularly since the amount of strain stored in the LC films can be modulated by either changing the thickness of the film or the temperature or composition of the lyotropic chromonic LC phase (in order to alter the magnitude of the elastic constants).[34,43]

Conclusions

In summary, our study reveals new dynamical behaviors of bacteria confined within thin homeotropic and hybrid nematic LC films, and provides insight into the origins of those behaviors. A key conclusion of our study is that elastic torques generated by the LC are sufficiently large to overcome wall-induced hydrodynamic torques, thus leading to LC-guided bacterial motion near surfaces that orient LCs. The dominating role of the elastic torques on the near-surface behaviors of the bacteria are evident in our studies with homeotropically aligned LCs (the bacteria adopted orientations perpendicular to the surface) and in hybrid aligned films (the bacteria followed the spatial variation in the director profile, thus exhibiting rectified motion). In addition, it is evident in comparisons of the behavior of swarm cells in LC films in the limit $L_{bacteria} > L_{film}$; as shown in Fig. 4, when the LC is aligned perpendicular to the surface, hydrodynamic interactions dominate the circular, in-plane motion of the cells because the LC exerts no torque (that influences in-plane motion); in contrast, when the LC is aligned in the plane of the surface, the LC-mediated torque results in trajectories of the cells that following the orientation of the director.

A second key conclusion of our study is that elastic stresses associated with non-uniform director profiles are sufficient to cause the deformation of the bacterial cell bodies when using long swarm cells. While we (Fig. 4) and others[58] have reported previously that hydrodynamic interactions can lead to changes in cell shape, the observations in Fig. 6 are the first to suggest that LC elastic stresses can deform cells. Indeed, our observations in Fig. 6 suggest that the cell body largely follows the director profile in LC films with hybrid anchoring. This coupling between cell shape and LC director profile suggests that descriptions of the dynamical behaviors of bacteria in LCs will, in general, need to consider the shape of the cells as a dependent variable of the system.

Overall, the findings reported in this paper also suggest the basis of new methods and approaches for manipulation of bacteria in technological contexts. For example, we show that rectification of bacteria motion is possible in hybrid LC films and that, unlike isotropic solution, this phenomenon is achieved in nematic LCs without the need for special geometric features present on the walls confining the fluid. Thus, it may represent a versatile new means to facilitate quantification and spatial localization of bacteria. Alternatively, by varying the

magnitude of the elastic stresses acting on elongated bacteria in hybrid films and determining the resulting configurations adopted by the cells, strained LCs might be used to report the mechanical properties of bacteria (*e.g.*, bending stiffness). In addition, we end by commenting that the dynamical response of the LC to the motions of bacteria (*e.g.*, the transient distortions of the LC produced by swarm cells moving in directions orthogonal to the LC director field) might also be used to measure physical properties of nematic LCs.

Conflict of interest

The authors declare the following competing financial interest(s): NLA declares a significant financial interest in Platypus Technologies LLC, a for-profit company that has developed LC-based technologies for molecular analysis.

Acknowledgements

References

1 J. C. Loudet, P. Hanusse and P. Poulin, *Science*, 2004, **306**, 1525.
2 F. Mondiot, J.-C. Loudet, O. Mondain-Monval, P. Snabre, A. Vilquin and A. Würger, *Phys. Rev. E: Stat., Nonlinear, Soft Matter Phys.*, 2012, **86**, 010401.
3 T. Turiv, I. Lazo, a. Brodin, B. I. Lev, V. Reiffenrath, V. G. Nazarenko and O. D. Lavrentovich, *Science*, 2013, **342**, 1351–1354.
4 M. D. Lynch and D. L. Patrick, *Nano Lett.*, 2002, **2**, 1197–1201.
5 C. Lapointe, A. Hultgren, D. M. Silevitch, E. J. Felton, D. H. Reich and R. L. Leheny, *Science*, 2004, **303**, 652–655.
6 U. Tkalec, M. Škarabot and I. Muševič, *Soft Matter*, 2008, **4**, 2402–2409.
7 F. Mondiot, S. P. Chandran, O. Mondain-Monval and J.-C. Loudet, *Phys. Rev. Lett.*, 2009, **103**, 238303.
8 B. Senyuk and I. I. Smalyukh, *Soft Matter*, 2012, **8**, 8729–8734.
9 I. Musevic, M. Škarabot, U. Tkalec, M. Ravnik and S. Žumer, *Science*, 2006, **313**, 954–958.
10 P. Poulin, H. Stark, T. C. Lubensky and D. A. Weitz, *Science*, 1997, **275**, 1770–1773.
11 M. Škarabot, M. Ravnik, S. Žumer, U. Tkalec, I. Poberaj, D. Babič, N. Osterman and I. Muševič, *Phys. Rev. E: Stat., Nonlinear, Soft Matter Phys.*, 2008, **77**, 031705.
12 M. Tasinkevych, F. Mondiot, O. Mondain-Monval and J.-C. Loudet, *Soft Matter*, 2014, **10**, 2047–2058.
13 A. Nych, U. Ognysta, I. Muševič, D. Seč, M. Ravnik and S. Žumer, *Phys. Rev. E: Stat., Nonlinear, Soft Matter Phys.*, 2014, **89**, 062502.
14 O. D. Lavrentovich, *Soft Matter*, 2014, **10**, 1264–1283.
15 C. P. Lapointe, T. G. Mason and I. I. Smalyukh, *Science*, 2009, **326**, 1083–1086.
16 B. Senyuk, J. S. Evans, P. J. Ackerman, T. Lee, P. Manna, L. Vigderman, E. R. Zubarev, J. van de Lagemaat and I. I. Smalyukh, *Nano Lett.*, 2012, **12**, 955–963.
17 S. P. Chandran, F. Mondiot, O. Mondain-Monval and J. C. Loudet, *Langmuir*, 2011, **27**, 15185–15198.
18 M. Škarabot, M. Ravnik, S. Žumer, U. Tkalec, I. Poberaj, D. Babič and I. Muševič, *Phys. Rev. E: Stat., Nonlinear, Soft Matter Phys.*, 2008, **77**, 061706.
19 V. G. Nazarenko, A. B. Nych and B. I. Lev, *Phys. Rev. Lett.*, 2001, **87**, 075504.
20 U. Tkalec, M. Ravnik, S. Čopar, S. Žumer and I. Muševič, *Science*, 2011, **333**, 62–65.
21 A. Kumar, T. Galstian, S. K. Pattanayek and S. Rainville, *Mol. Cryst. Liq. Cryst.*, 2013, **574**, 33–39.
22 P. C. Mushenheim, R. R. Trivedi, H. H. Tuson, D. B. Weibel and N. L. Abbott, *Soft Matter*, 2014, **10**, 88–95.
23 S. Zhou, A. Sokolov, O. D. Lavrentovich and I. S. Aranson, *Proc. Natl. Acad. Sci. U. S. A.*, 2014, **111**, 1265–1270.
24 P. C. Mushenheim, R. R. Trivedi, D. B. Weibel and N. L. Abbott, *Biophys. J.*, 2014, **107**, 255–265.
25 A. Sokolov, S. Zhou, O. D. Lavrentovich and I. S. Aranson, *Phys. Rev. E: Stat., Nonlinear, Soft Matter Phys.*, 2015, 013009.
26 T. Shaw, M. Winston, C. J. Rupp, I. Klapper and P. Stoodley, *Phys. Rev. Lett.*, 2004, **93**, 098102.
27 H.-C. Flemming and J. Wingender, *Nat. Rev. Microbiol.*, 2010, **8**, 623–633.
28 P. Y. Tam, D. F. Katz and S. A. Berger, *Biorheology*, 1980, **17**, 465–478.
29 S. J. Haward, J. A. Odell, M. Berry and T. Hall, *Rheol. Acta*, 2011, **50**, 869–879.
30 A. Berke, L. Turner, H. Berg and E. Lauga, *Phys. Rev. Lett.*, 2008, **101**, 038102.
31 E. Lauga and T. R. Powers, *Rep. Prog. Phys.*, 2009, **72**, 096601.
32 H. H. Tuson, M. F. Copeland, S. Carey, R. Sacotte and D. B. Weibel, *J. Bacteriol.*, 2013, **195**, 368–377.
33 D. M. Agra-Kooijman, G. Singh, A. Lorenz, P. J. Collings, H.-S. Kitzerow and S. Kumar, *Phys. Rev. E: Stat., Nonlinear, Soft Matter Phys.*, 2014, **89**, 062504.
34 S. Zhou, A. J. Cervenka and O. D. Lavrentovich, *Phys. Rev. E: Stat., Nonlinear, Soft Matter Phys.*, 2014, **90**, 042505.
35 Y. A. Nastishin, H. Liu, S. V. Shiyanovskii, O. D. Lavrentovich, A. F. Kostko and M. A. Anisimov, *Phys. Rev. E: Stat., Nonlinear, Soft Matter Phys.*, 2004, **70**, 051706.
36 J. V. Champion and G. H. Meeten, *J. Pharm. Sci.*, 1973, **62**, 1589–1595.
37 S. S. Roy, D. J. Bindl and M. S. Arnold, *J. Phys. Chem. Lett.*, 2012, **3**, 873–878.
38 X. Li, Y. Zhu, W. Cai, M. Borysiak, B. Han, D. Chen, R. D. Piner, L. Colombo and R. S. Ruoff, *Nano Lett.*, 2009, **9**, 4359–4363.

39 J. Jeong, G. Han, A. T. C. Johnson, P. J. Collings, T. C. Lubensky and A. G. Yodh, *Langmuir*, 2014, **30**, 2914–2920.

40 F. D. Bloss, *An Introduction to the Methods of Optical Crystallography*, Holt, Rinehart and Winston, New York, 1961.

41 C. J. Smith and C. Denniston, *J. Appl. Phys.*, 2007, **101**, 014305.

42 I. I. Smalyukh, J. Butler, J. D. Shrout, M. R. Parsek and G. C. L. Wong, *Phys. Rev. E: Stat., Nonlinear, Soft Matter Phys.*, 2008, **78**, 030701.

43 S. Zhou, K. Neupane, Y. A. Nastishin, A. R. Baldwin, S. V. Shiyanovskii, O. D. Lavrentovich and S. Sprunt, *Soft Matter*, 2014, **10**, 6571–6581.

44 H. Stark and D. Ventzki, *Phys. Rev. E: Stat., Nonlinear, Soft Matter Phys.*, 2001, **64**, 031711.

45 K. Drescher, K. C. Leptos, I. Tuval, T. Ishikawa, T. J. Pedley and R. E. Goldstein, *Phys. Rev. Lett.*, 2009, **168101**, 1–4.

46 A. P. Petroff, X.-L. Wu and A. Libchaber, *Phys. Rev. Lett.*, 2015, 158102.

47 G. Lowe, M. Meister and H. C. Berg, *Nature*, 1987, **325**, 637–640.

48 A. D. Rowe, M. C. Leake, H. Morgan and R. M. Berry, *J. Mod. Opt.*, 2003, **50**, 1539–1554.

49 S. Chattopadhyay, R. Moldovan, C. Yeungt and X. L. Wu, *Proc. Natl. Acad. Sci. U. S. A.*, 2006, **103**, 13712–13717.

50 J. Fukuda, B. I. Lev and H. Yokoyama, *J. Phys.: Condens. Matter*, 2003, **15**, 3841–3854.

51 M. Vilfan, N. Osterman, M. Čopič, M. Ravnik, S. Žumer, J. Kotar, D. Babič and I. Poberaj, *Phys. Rev. Lett.*, 2008, **101**, 237801.

52 J. Fukuda and S. Žumer, *Phys. Rev. E: Stat., Nonlinear, Soft Matter Phys.*, 2009, **79**, 041703.

53 M. Kleman and O. D. Lavrentovich, *Soft Matter Physics: An Introduction*, Springer-Verlag, New York, 2003.

54 E. Lauga, W. R. DiLuzio, G. M. Whitesides and H. A. Stone, *Biophys. J*, 2006, **90**, 400–412.

55 P. Galajda, J. Keymer, P. Chaikin and R. Austin, *J. Bacteriol.*, 2007, **189**, 8704–8707.

56 S. E. Hulme, W. R. DiLuzio, S. S. Shevkoplyas, L. Turner, M. Mayer, H. C. Berg and G. M. Whitesides, *Lab Chip*, 2008, **8**, 1888–1895.

57 L. D. Landau and E. M. Lifshitz, *Theory of Elasticity*, Pergamon Press, 3rd edn, 1986.

58 A. Amir, F. Babaeipour, D. B. Mcintosh, D. R. Nelson and S. Jun, *Proc. Natl. Acad. Sci. U. S. A.*, 2014, **111**, 5778–5783.